DLP-printable fully biobased soybean oil composites

# DLP-printable fully biobased soybean oil composites

**Camilla Noè[1], Andrea Cosola[1], Chiara Tonda-Turo[2], Raffaella Sesana[2], Cristiana Delprete[2], Annalisa Chiappone[1], Minna Hakkarainen[4] and Marco Sangermano[1*]**

[1]Politecnico di Torino, Dipartimento di Scienza Applicata e Tecnologia C.so Duca Degli Abruzzi 24, 10129 Torino, Italy; camilla.noe@polito.it; andrea.cosola@polito.it; annalisa.chiappone@polito.it, marco.sangermano@polito.it

[2]Politecnico di Torino, Dipartimento di Ingegneria Meccanica e Aerospaziale, C.so Duca Degli Abruzzi 24, 10129 Torino, Italy; chiara.tondaturo@polito.it, raffalla.sesana@polito.it, cristiana.delpete@polito.it

[3]Politecnico di Torino Institute of Materials Physics and Engineering, Department of Applied Science and Technology, Torino, Italy; sergio.perero@polito.it

[4] KTH Royal Institute of Technology, Department of Fibre and Polymer Technology, 100 44 Stockholm, Sweden; minna@kth.se

## Abstract

Composites reinforced with micro-particles are widely used in engineering fields. Unfortunately, the traditional manufacturing processes do not allow customization and shape complexity achievable with additive manufacturing technologies. In particular, VAT polymerization enables the highest printing resolution. Here, we demonstrate the fabrication of fully-biobased composites consisting of a matrix of acrylated soybean oil (ASO) and a lignocellulose waste derived from the macadamia nut industry (macadamia nut-shell, MAC) as reinforcing agent. Different formulations were prepared by varying the content of MAC, and their reactivity was evaluated by means of Fourier transform infrared spectroscopy and photorheology. The suitability of the formulated novel biobased inks for digital light processing (DLP) 3D-printing was illustrated by successful

printing of complex 3D-structures with a high resolution. The thermo-mechanical and mechanical properties of the 3D-printed composites were tested by DSC, DMTA and tensile tests, which revealed that. increasing MAC contents reflected into higher glass transition temperatures, ranging from 25 to 46°C, and higher Young's modulus, ranging from 15 to 100 MPa. The morphology of the samples and the dispersion of the MAC in the ASO network was investigated by field emission scanning electron microscopy, while the surface roughness of the printed composites was analysed with profilometry. Cytotoxicity, cell adhesion and cell proliferation tests with human fibroblast cells were carried out in view of the fabrication of scaffolds for bioengineering and the results envisage good potential for these fully bio-based composites in the biomedical field.

**Keywords**

Renewable materials, soybean oil, biobased composites, DLP-printing

## 1. Introduction

The design of organic-inorganic materials has inspired researchers to model a new generation of composites for additive manufacturing (AM). Indeed, AM stands out over the traditional manufacturing processes used for composite materials since it allows to rapidly obtain customized objects with high shape-complexity, while minimizing material consumption and avoiding extra tooling costs. For those reasons, the global market of materials for AM is increasing exponentially, and it is likely to overcome 23 billion dollars in 2029 [1]. Among all the AM-technologies, VAT-polymerization technology (VP), a light-based AM technology, allows to achieve the highest printing resolution and the highest object complexity [2]. However, despite the abovementioned advantages, the

applicability of VP is restricted by the limited availability of sustainable photopolymerizable resins [3]. Indeed, the vast majority of the commercially available 3D printable photopolymers involve acrylates and epoxides derived from fossil fuel resources. However, the increasing environmental concern and the progressive fossil fuel depletion are driving the research to develop "green" alternatives [4–8].

Among them, vegetable oils (VOs) are the most widely investigated natural materials for the development of biobased photocurable resins, due to their abundant availability and low cost, low-toxicity, biodegradability. They also contain several reactive sites which can be substituted with photopolymerizable functionalities via epoxidation or (meth)acrylation reactions, which gives the opportunity to prepare VO-based photocurable resins. [9–13].

VOs are triglycerides made of three fatty acids joined together through a glycerol unit. One of the most commonly produced VOs is the one extracted from soybean seeds (i.e. soybean oil), which is characterized by the presence of several unsaturated groups along the main chain, suitable for epoxidation and following (meth)acrylation [14].

In 2016, the use of acrylated soybean oil (ASO) has been firstly reported for stereolithography (SLA) applications, aiming to produce biocompatible scaffolds [15]. Later, ASO and vanillin dimethacrylate/diacrylate were combined successfully as inks for direct laser printing [16]. Also, methacrylated soybean oil with additional functionalities was used with other biobased diluents to prepare photocurable resins for digital light processing (DLP) [17]. Furthermore, soybean oil was combined with sucrose to prepare a novel biobased formulation for SLA [18]. Even if the processing of VOs via VP has been successfully demonstrated, the mechanical properties of the printed parts

were generally quite poor. To solve this problem and with the aim to extend the possible applications fields of 3D-printed VOs, fillers can be added [19,20]. However, the addition of bio-based fillers as reinforcing agents in VP 3D printing was rarely investigated compared to fused deposition modeling 3D printing [21,22]. In fact, the VP-related works focused only on lignin, cellulose, chitosan and chitin nanocrystals or nanofibrils [4].

Macadamia nutshell (MAC) is a lignocellulose-rich agricultural waste deriving from the macadamia nut production, accounting for 44000 metric tons per year [23–25]. The end-of-life of MAC mainly involves landfilling or incineration, hence leading to environmental pollution, greenhouse gas emissions and waste of valuable resources. Moreover, MAC particles have been previously used as reinforcement to generate acrylonitrile-butadiene-styrene composite filaments for fusion deposition modelling [26]. ~~We anticipated that~~ Therefore, we selected MAC powder ~~could be utilized~~ as a reinforcing renewable filler for ASO matrix to fabricate fully biobased composites via DLP-printing. The incorporation of MAC powder in a biobased matrix could enhance the value of this bio-renewable feedstock and lead to environmental benefits.

The effect of MAC powder on the kinetics of polymerization, mechanical and thermal properties of the resulting thermoset composites was investigated in detail. Moreover, cell viability and cell proliferation tests using human fibroblasts cells (HHF-1, ATCC) were performed to assess the potential of these printed biobased thermosets composites as competitive and sustainable scaffolds for bioengineering applications. This work gives an insight on the 3D printing of bioscaffolds with renewable biocomposites.

## 2. Materials and methods

### 2.1 Materials

Acrylated soybean oil (ASO) (density = 1.04 g/mL at 25°C, $M_w$ = 1200 g/mol, 3.4 acrylates per trigliceride) [27], dimethyl sulfoxide (DMSO) (ACS reagent P99.9%), ethanol absolute, and bis-(2,4,6-trimethylbenzoyl) phenylphosphine oxide (BAPO) were purchased by Sigma Aldrich (Milano, Italy). The macadamia nut shell (MAC) was obtained from the 814 variety of macadamia (density 721.34 ± 87.07 kg/m$^3$, the average particles dimensions was 140 μm as evaluated by FESEM images) [28,29].

### 2.2 Biobased composites preparation

The photocurable formulations were prepared by dispersing different amounts of MAC into ASO liquid. ~~After stirring~~ The formulations were subsequently placed on a magnetic stirring plate (300 rpm, T=25°C). After ~~for~~ 5 min of stirring 1 phr of the photoinitiator BAPO was added along with 5 phr of ethanol to allow a complete dispersion of the phI into the ASO. ~~to~~ Then the formulations were stirred for additionally 10 minutes (Tab.1).

**Tab. 1**. Composition of the photocurable ASO formulations

| Formulations | ASO [%wt] | MAC [%wt] | BAPO [phr] |
|---|---|---|---|
| ASO | 100 | 0 | 1 |
| ASO-MAC1 | 99 | 1 | 1 |
| ASO-MAC5 | 95 | 5 | 1 |
| ASO-MAC10 | 90 | 10 | 1 |

### 2.3 Digital light processing 3D printing

The ASO composites were 3D-printed using a commercial DLP printer from ASIGA (MAX X, light emission at λ= 385 nm, nominal xy-pixel resolution of 27 μm) The UV light intensity and the layer thickness were set to 32 mW/cm$^2$ and 50 μm, respectively,

while the exposure time/layer was optimized for each formulation based on the preliminary photorheology investigations. Lastly, the printed objects were sonicated in ethanol for 1 min to remove the unreacted monomers and then post-cured under UV-light using a medium-pressure mercury lamp provided by Robot Factory (2 min, 12 mw/cm$^2$).

## 2.4 Evaluation techniques

### 2.4.1 Fourier Transform Infrared Spectroscopy (FTIR)

The FTIR spectra of ASO and ASO composites were recorded by Nicolet iS 50 Spectrometer FTIR spectrometer (Perkin Elmer, Norwalk, CT, USA) in transmission mode. For each sample, 16 scans were recorded with 4 cm$^{-1}$ resolutions. Data were processed using the software Omnic from Thermo Fisher Scientific. The double bond conversion was calculated by following the decrease of the double peaks centred at 1636-1618 cm$^{-1}$. The double peak at 1740-1727 cm$^{-1}$ representing the C=O bond stretching vibration of the triglycerides was utilized as internal standard, since it is not affected by the reaction. The calculation was done according to Eq. 1.

$$Conversion\ (\%) = \left(1 - \frac{\frac{A_{C=C,post}}{A_{C=C,pre}}}{\frac{A_{ref,post}}{A_{ref,pre}}}\right) * 100 \qquad (1)$$

Where $A_{C=C,pre}$ and $A_{C=C,post}$ represent the area of the double bond peak before and after the photopolymerization reaction, respectively and $A_{ref,pre}$ and $A_{ref,post}$ represent are the area of the reference peak before and after the photopolymerization reaction.

### 2.4.2 Photorheology

The photorheology tests were performed with an Anton PAAR Modular Compact Rheometer (Physica MCR 302, Graz, Austria) using a parallel plate configuration ($\phi$= 15

mm) with a quartz bottom glass. The gap value was set as 300 μm. All experiments were carried out at T = 25°C. Oscillatory rheometer operating in time and stress sweep modes was used to monitor the viscoelastic properties associated with the crosslinking kinetics. The time sweep experiment was performed in the linear viscoelastic region (LVR) at a constant strain amplitude (λ) of 0.5% and a constant angular frequency (ω) of 6 rad/s to monitor the crosslinking reaction by following the evolution of elastic storage modulus G' with time. After 30 s, the UV Hamamatsu LC8 lamp (Hamamatsu City, Japan) with a light intensity of 28 mW cm-1 was turned on. The samples were irradiated from the bottom.

#### 2.4.3 Optical microscopy

The surfaces of the 3D-printed ASO composites were monitored with an Olympus BX53 M optical microscope. The ocular lenses and the objective lenses were equipped with 10× magnification.

#### 2.4.4 Gel content percentage (G%)

The gel content percentage (G%) of the cured composites was determined by measuring the weight loss after 24 h extraction with chloroform. G% was calculated according to Eq. (2):

$$G\% = \frac{W_i}{W_0}\, x\, 100\% \qquad (2)$$

where $Wi$ is the weight of the dry sample after the treatment with chloroform and $W_0$ is the weight of the dry sample before the treatment.

#### 2.4.5 Dynamic thermal-mechanical analysis (DMTA)

DMTA analysis was performed with a Triton Technology - Tritec 2000 DMA. Samples were cooled with liquid nitrogen and measurements were run with a heating rate of 3 °C

$min^{-1}$ in tensile mode. The frequency used was 1 Hz. The samples dimensions were 12 mm x 6 mm x 0.2 mm.

### 2.4.6 Differential scanning calorimetry (DSC)

DSC analyses were performed by using a Mettler Toledo DSC instrument. Approximately 10 mg of each sample were insert in a 100 µl aluminium pans with pierced lids in an inert atmosphere ($N_2$, 50 ml $min^{-1}$). Thermal behaviour of the samples was investigated by using two repeated heating-cooling cycles. The temperature program was: first ramp from -60 °C to 150 °C, followed by a cooling cycle from 150 °C to -60 °C. After an isotherm at -60 for 10 min, a second heating cycle was performed from -60 to 150°C. The applied heating rate was 10 °C $min^{-1}$. Glass transition temperature (*Tg*) was determined from the second heating curve.

### 2.4.7 Tensile Testing

Tensile tests were performed on rectangular specimens ($w$ x $l$ x $t$ =10 x 50 x 2 mm) according to ASTM D1708-18 [30] using MTS QTestTM/10 Elite controller (MTS Systems Corporation, Edan Prairie, Minnesota, USA) using TestWorks® 4 software (Edan Prairie, Minnesota, USA). The tensile force was applied parallel to the samples axis at a constant cross-head displacement rate of 2 mm/min. The strain was measured as the ratio between cross-head displacement and the initial distance between the grips. The tress was calculated as the ratio between the force and the cross-section area. The Young's modulus ($E$) of each sample was calculated from the slope of the initial linear portion of the stress–strain curve. The toughness of the materials was calculated by calculating the area underneath the stress–strain curves. Three samples for each material composition were tested.

### 2.4.8 Field Emission Scanning Electron Microscopy (FESEM)

The morphological characterization of the ASO composites was performed by using a FESEM Zeiss Supra 40 (Oberkochen, Germany). Before the analysis, the samples were covered with a 7nm thick film of Platinum.

### 2.4.9 Cell Viability

Cytotoxicity tests were performed following the ISO10933-5 for indirect tests to identify any cytotoxic events due to release of compounds from the ASO and ASO-MAC hydrogels. Conditioned media were prepared by soaking 0.1 g of ASO and ASO-MAC samples into 1 mL of complete medium (Dulbecco's Modified Eagle's Medium, 15% fetal bovine serum, 1% penicillin streptomycin). Two conditions were tested: samples were soaked for 24 hours (conditioned medium_24h) and for 7 days (conditioned medium_7d). Human fibroblasts (HFF-1 ATCC® cells) were cultured in a 96-plate multiwell (MW96) using a cell density of $2\times10^4$ cells/well. After 24 h, the cells reached confluence and culture medium was removed from each well and substituted with conditioned medium (conditioned medium_24h or conditioned medium_7d). Control samples (CTRL) were prepared by substituting the medium with not-conditioned fresh medium. After 24 h, the medium was substituted in each well with 100 µL of 0.1 mg/mL non-fluorescent resazurin solution in phosphate buffered saline-PBS. Cell viability was measured as non-fluorescent resazurin is converted to fluorescent resorufin by cell metabolism and the fluorescent signal was monitored using a plate reader (Biotek) at 530 nm excitation wavelength and 590 nm emission wavelength. Experiments were performed using six samples for each condition and cell viability was calculated as a percentage value compared to CTRL.

### 2.4.10 Cell Adhesion and Proliferation

Direct assays were performed to assess the adhesion and proliferation ability of HFF-1 cells on ASO and ASO-MAC grid-shaped samples. ASO and ASO-MAC grids 3D printed as previously described, after which they were blocked at the bottom of MW48 plate to avoid floating and seeded with $2\times10^4$ cells/well. Briefly, a drop of 50µl containing $2\times10^4$ cells was placed on the top of each grid and incubated for 2 hours, after which 450 µl of fresh media were added. At different time points (1, 3 and 7 days), cell viability was measured using resazurin as previously described. To avoid an overestimation ascribed to cells adhered at the bottom of the plate, samples were placed in a new MW48 before adding the resazurin solution. Furthermore, cell morphology was assessed through immunostaining. Firstly, cells were fixed with 4% paraformaldehyde for 30 minutes, permeabilized with 0.5% TRITON-X in PBS for 10 minutes and blocked with 1% (w/v) bovine serum albumin (BSA, Sigma-Aldrich) in PBS for 30 minutes. Then, nuclei and actin filaments were stained incubating samples in a DAPI solution (1:1000 in PBS, Thermofisher Scientific) and rhodamine phalloidin solution (1:60 in PBS, Thermofisher Scientific) for 10 and 40 minutes, respectively.

## 2. Result and discussion

Fully biobased composites were produced via photoinduced radical polymerization, using ASO (Scheme 1) as photopolymerizable matrix, and macadamia nutshell as bio-reinforcement (see the experimental section for detailed information on the final composition of the photocurable system).

**Scheme 1**: ASO chemical structure.

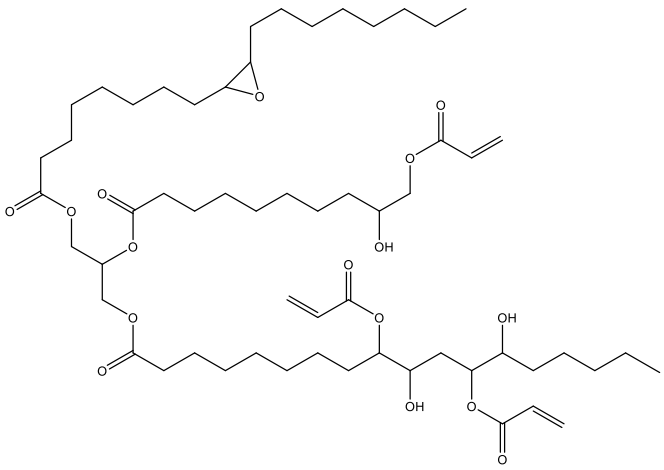

The characterization of the ASO resin was performed through FTIR analysis. Fig.1 shows the ASO spectra before and after the UV irradiation. In the spectra, there can be clearly seen the characteristic peaks of ASO. The broad peak at 3468 $cm^{-1}$ represents the -OH groups vibration while the bands at 2927 and 2855 $cm^{-1}$ represent the asymmetrical and symmetrical stretching of C-H methylene groups; the signals at 1740-1727 $cm^{-1}$ and 1190 $cm^{-1}$ are assigned to the C=O and C-O groups vibration in triglycerides, respectively. while the small peak at 720 $cm^{-1}$ is attributed to the cis-CH=CH group vibrations.

**Fig. 1**: ASO FTIR spectra before and after the UV irradiation.

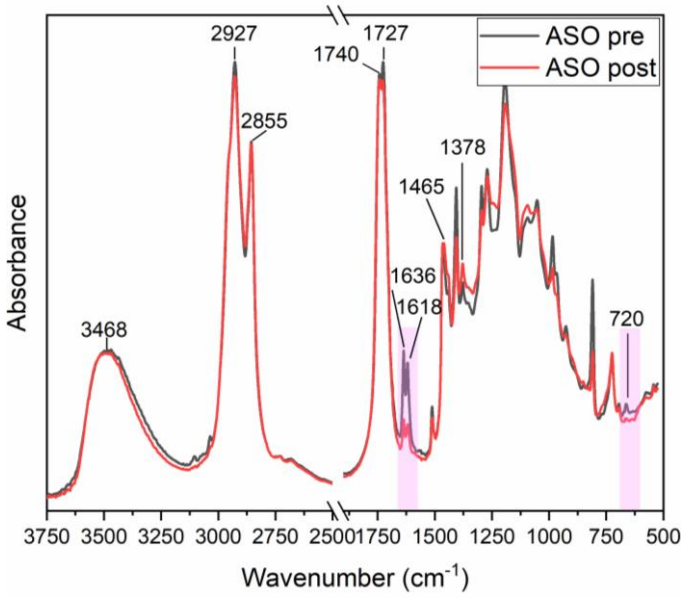

By means of FTIR analysis, it was also possible to monitor the photopolymerization reaction,~~The photopolymerization reaction was monitored by means of IR spectroscopy,~~ following the intensity of the peak at 1636 and 1618 which are ascribed to the stretching vibrations of carbon-carbon double bonds (C=C) of ASO. ~~A detailed description of the FTIR peaks is reported in the supporting information.~~

As it can be noticed by comparing the spectra of ASO collected before and after the photopolymerization (Fig.1~~,a~~) the C=C signals markedly decreased, confirming the photocrosslinking. Moreover, the photopolymerization kinetic was first studied monitoring the evolution of the double bond conversion (DBC) over time. For this purpose, FTIR spectra were recorded at different irradiation times (10, 20, 30, 40, 50 and 60 s). The obtained plots (DBC vs time) are shown in Fig.2,a~~S1~~. Overall, all the investigated formulations showed fast reactivity, reaching high DBC values (> 85%, see Tab. 2) in less than 30 seconds of irradiation. This indicates the high reactivity of the bio-based arylated resin.

The kinetic of photopolymerization of the ASO-MAC mixture was also investigated by means of real-time photorheology, which monitors any changes in viscoelastic properties of the material during light-irradiation. Fig.2~~-1~~,b shows the storage moduli (G') of the ASO-MAC samples vs irradiation time.

These results further confirmed the high reactivity of the photocurable system. Indeed, as evidenced by the fast increase of G', the photopolymerization is rapidly activated once the light irradiation is switched on.

In particular, both the pristine formulation and those ones containing 1wt% and 5wt% of MAC reached the G' plateau in 30 seconds. The fast reactivity of these formulations is comparable to the one previously obtained for poly(lactide-*co*-glycolide) (PLGA)

diacrylates inks applied for the generation of bioscaffolds [31]. When the MAC percentage was increased to 10wt% a longer irradiation time is needed to reach the G' plateau (90 s). However, a gradual decrease in the photopolymerization kinetics, calculated as the slope of the G' curves ($\Delta G'/\Delta t$), was already observed when 1wt% or 5wt% of MAC was added. Indeed $\Delta G'/\Delta t$ gradually decreased from 56 to 28 $kPa*s^{-1}$ as the MAC concentration increased, confirming the slowdown-effect induced by the presence of MAC. This can be probably attributed to the UV-shielding effect of MAC, the colour of which causes a marked reduction of the formulation transparency thus limiting the light penetration. The slight reduction in the photoreactivity of the system when adding MAC is consistent with both the slight decrease of the DBC recorded by the FTIR (data reported in Tab.2 with a DBC decrease from 89 to 85%) and with the moderate lowering of the insoluble fraction of the composites revealed by the gel content measurements (Tab.2).

Moreover, the photorheology curves also revealed that the G' values at plateau slightly increased with higher MAC content (from 4 MPa of pristine ASO to 11 MPa of ASO-MAC10). This suggests that MAC may act as reinforcing agent in the ASO matrix.

**Fig. 2**: a) Evaluation of the DBC of ASO and ASO composites at different irradiation times.; b) photorheology curves.

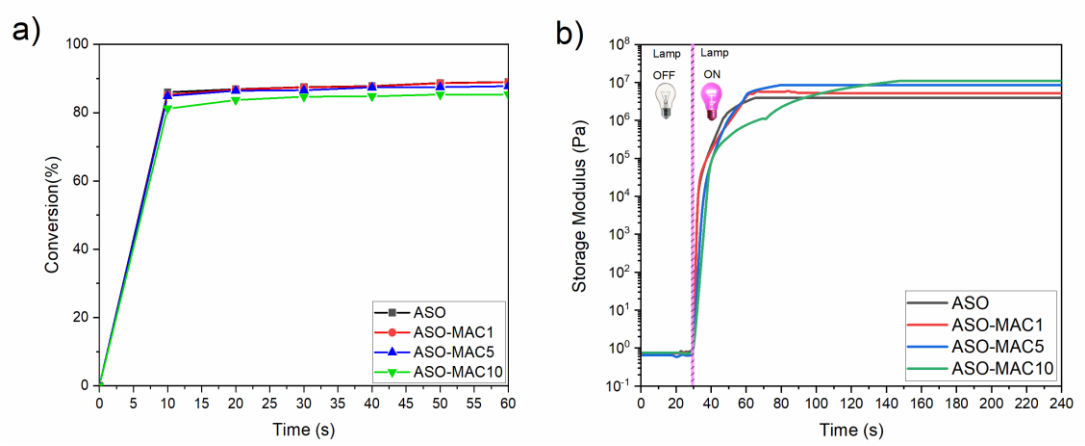


**Tab. 2.** Characterization of the crosslinking parameters of ASO formulations.

| | ASO | ASO-MAC1 | ASO-MAC5 | ASO-MAC10 |
|---|---|---|---|---|
| FTIR Conversion [%] | 89 | 89 | 87 | 85 |
| $\Delta G'/\Delta t$ [kPa $s^{-1}$] | 56 | 44 | 29 | 28 |
| Gel [%] | 90 | 87 | 86 | 85 |

Once the high reactivity of the formulations was proven, we investigated their suitability as novel biobased inks for DLP-printing. Based on the kinetic data observed via photorheology, the printing parameters were optimized for each formulation. In particular, the exposure time/layers was varied between 1s and 2.5s with increasing MAC content. Expectations were confirmed since complex computer aided design (CAD) 3D-models could be successfully reproduced with a high resolution from all the ASO-MAC formulations.

Interestingly, the presence of MAC as coloured filler enabled printing complex geometries displaying a high fidelity to the original CAD models without UV-light shielding effect typically induced by the presence of dark fillers [32,33]. ~~the need of dye addition, which is typically required to limit light diffusion in the vat and over-polymerization phenomena.~~ All the printed objects were post-cured with a low-intensity medium-pressure lamp washed with ethanol to both minimize the C=C bond amount and to remove unreacted and cytotoxic products. These steps are highly recommended for biocompatible material as previously reported in the literature especially in the case of acrylates [34–36]. Fig.2,a presents examples of ASO, ASO-MAC1, ASO-MAC5and ASO-MAC10 3D-printed objects reproduced from the same digital model, while (Fig.2,b) shows a complex lattice-shaped structure printed with ASO-MAC10. The high fidelity of the printed objects with the original CAD file was assessed with optical microscopy as shown in the Fig.2,c.

**Fig. 3**. a) example of ASO, ASO-MAC1, ASO-MAC5and ASO-MAC10 3D-printed composites; b) complex lattice-shaped structure from ASO-MAC10; c) fidelity evaluation of the printed objects with optical microscopy.

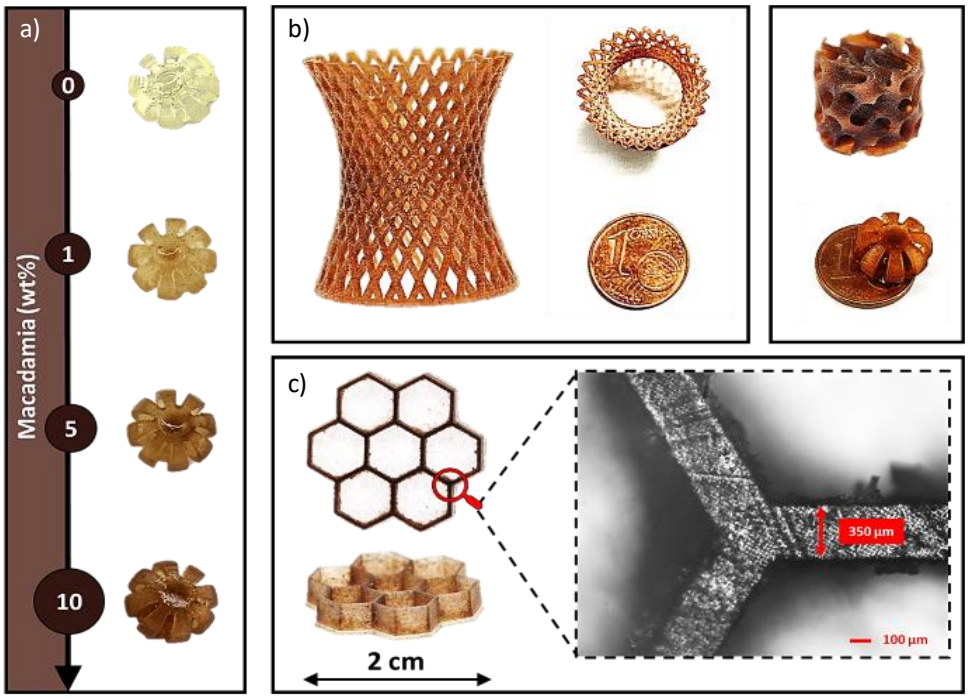


Dynamic-mechanical thermal analysis (DMTA) was carried out to investigate the thermomechanical properties of the printed composites. Fig.3,a reports the tanδ curve and the storage modulus (E') of the ASO-based specimens as a function of the temperature. The results revealed that the Tg of the composites, measured as the maximum of the tanδ plot, increased with higher MAC content (Tab.3). The same trend was confirmed also by DSC analyses), indicating that MAC particles behave as effective reinforcing agents for the ASO matrix. Besides, the flattening and broadening of the tanδ curves can be attributed to the formation of heterogeneous networks, characterized by a wide distribution of chain mobilities and relaxations time [5,37]. Moreover, in Fig.3,a, the increase of the E' values in the rubbery plateau region as a function of MAC content, is

likely explained by the presence of microparticles which act as a physical barriers reducing the mobility of the ASO chains [38].

The mechanical properties were further investigated by means of tensile measurements.

The average stress-strain curve of the ASO composites are given in Fig.3,b and in Tab.3. The ultimate tensile strength (UTS) and the Young's modulus (*E*) of the composites significantly increased with higher MAC content reaching the maximum UTS and a Young's modulus of 3.8 MPa and 100 MPa, respectively, in the case of ASO-MAC10. These results were expected, since the Young's modulus of a composite generally increases with the addition of a reinforcing agent. The obtained Young's modulus values are similar the one reported for 3D printed polycaprolactone (20 MPa) and for polylactic acid/multi-wall carbon nanotubes/polyethylene glycol composites (26 MPa) applied in bone tissue engineering [39,40].

The addition of MAC increased the toughness of the composites, defined as the ability of the material to absorb energy before fracture, from 1 to 7 MJ. Interestingly the young's modulus values of the ASO-based composite here presented, ranging from 15 to 100 MPa, match with the values typically reported for the human bone tissues [30]. This may envisage the potential use of these biobased composites for the preparation of DLP-printed scaffold for bone tissue engineering applications.

Moreover, the elongation at break ($\varepsilon_b$) of all the prepared composites were similar or slightly higher compared with the samples prepared without addition of MAC (Tab.3). The highest value was reached with 1wt% of MAC (5.5%). The $\varepsilon_b$ is influenced by complex phenomena, which may include filler/matrix interface properties, filler shape and/or distribution and variable viscoelastic properties of the matrix. The maintenance or even slight increase in $\varepsilon_b$ after MAC addition likely reflects good filler/matrix adhesion.

**Fig. 4.** a) DMTA analysis and b) Tensile test of ASO and ASO composites.

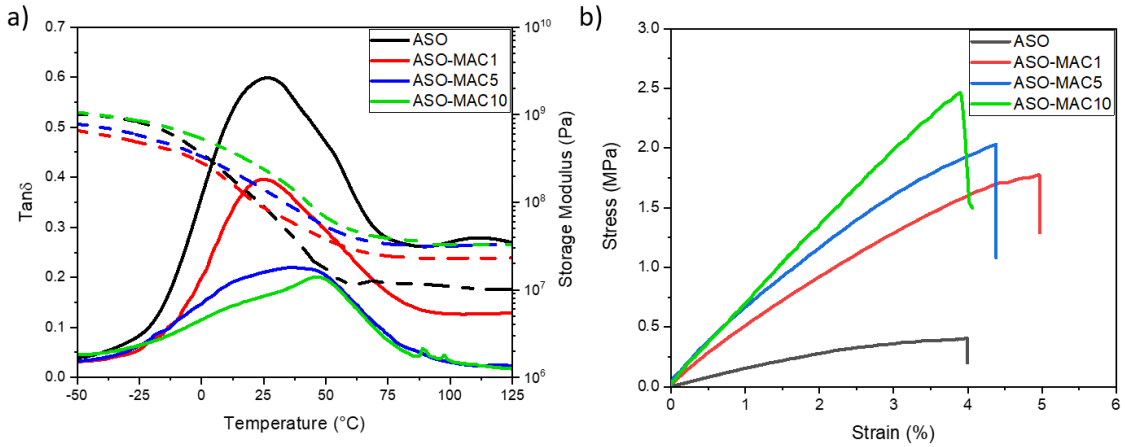


**Tab. 3**. Thermal and mechanical properties of ASO and ASO composites

| Sample | Tg_DMTA [°C] | E_rubbery [MPa] | Tg_DSC [°C] | *E* [MPa] | UTS [MPa] | $\varepsilon_b$ [%] | $K_{IC}$ [MJ/m$^3$] |
|---|---|---|---|---|---|---|---|
| ASO | 25 | 12.0 | 10 | 15.0±0.2 | 0.45±0.07 | 4.0±0.3 | 1.28±0.1 |
| ASO-MAC1 | 27 | 24.1 | 15 | 54.3±0.2 | 1.80±0.15 | 5.5±0.4 | 6.57±1.2 |
| ASO-MAC5 | 38 | 31.3 | 22 | 68.5±0.5 | 1.98±0.24 | 4.9±1.1 | 6.61±1.8 |
| ASO-MAC10 | 46 | 33.0 | 30 | 100.2±1.7 | 3.80±0.40 | 4.5±0.9 | 7.01±2 |

The morphology of composites was also studied by field-emission scanning electron microscopy (FESEM). Fig.4 reports the micrographs of the fractured surfaces of the composites. A good dispersion of the MAC microparticles within the matrix was achieved in the case of ASO-MAC1, while with higher MAC concentration a certain number of agglomerates can be noticed, which is even more evident in the ASO-MAC10 composite. All the composites show rough fracture surfaces, which indicates a high resistance to crack propagation [31].

**Fig. 5.** FESEM micrographs of a) ASO, b) ASO-MAC1, c) ASO-MAC5 and d) ASO-MAC10 composites.

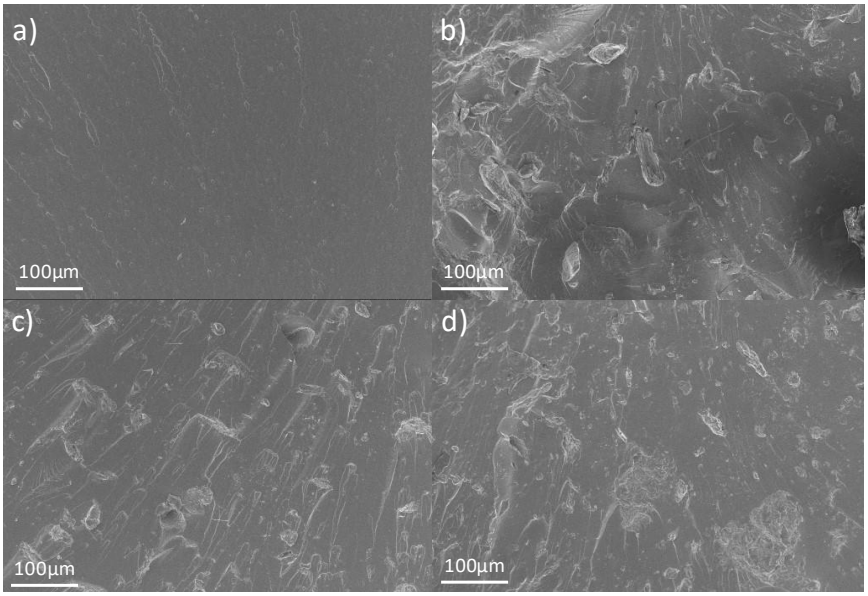


Cell viability

Direct and indirect tests were conducted to assess the ability of ASO-MAC samples to act as substrates for cell adhesion and proliferation. No cytotoxic effects were observed through indirect tests indicating that ASO and ASO-MAC samples did not induce cell death by the release of photoinitiator or unreacted polymer chains or degradation products within the first day (conditioned medium_1d) and up to 7 days (conditioned medium_7d) (Fig.5,A). The adhesion and proliferation of HFF-1 cells on ASO-MAC samples revealed no significant differences among the samples loaded with different MAC contents (Fig.5 ,B). Although, the MAC amount did not affect adhesion and proliferation, a slight reduction in cell number compared to control was observed at each time point. The 2D surface utilized as control offered a higher area compared to the grid-shaped samples (filament/pore ratio 2,5) increasing the number of adhered cells and consequently the proliferation rate at the different time points. Furthermore, the ability of the proposed

biobased composites to support cell colonization was confirmed through immunostaining at 7 days (Fig.6). HFF-1 shows a spread morphology of the cells when adhered on the grid filaments and a uniform cell distribution.

**Fig. 6**. HFF-1 cell viability: A) indirect tests at two conditions: samples were soaked for 24 hours (conditioned medium_24h) and for 7 days (conditioned medium_7d) and B) proliferation assay at 1, 3 and 7 days using printed grid-shaped samples.

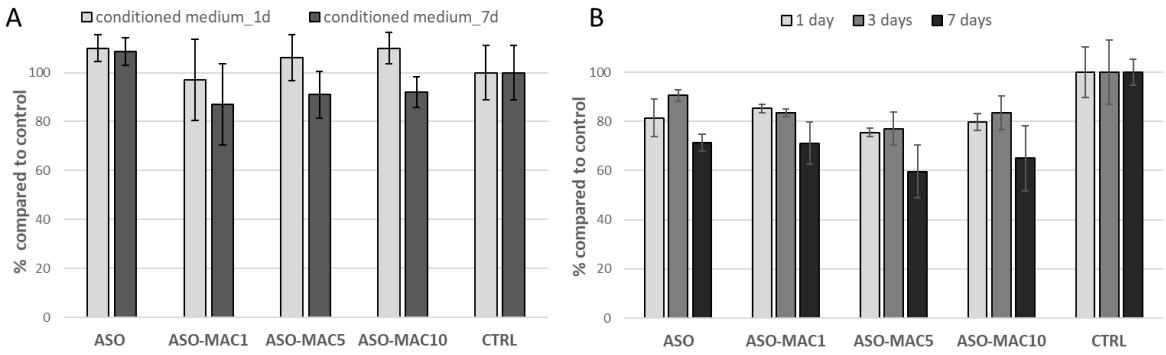

**Fig. 7.** Nuclei and actin filaments staining of ASO and ASO-MAC grid-shaped samples. Polystyrene plates were used as control (CTRL). A slightly blue autofluorescence can be observed for ASO samples. Scale bar: 50 µm.

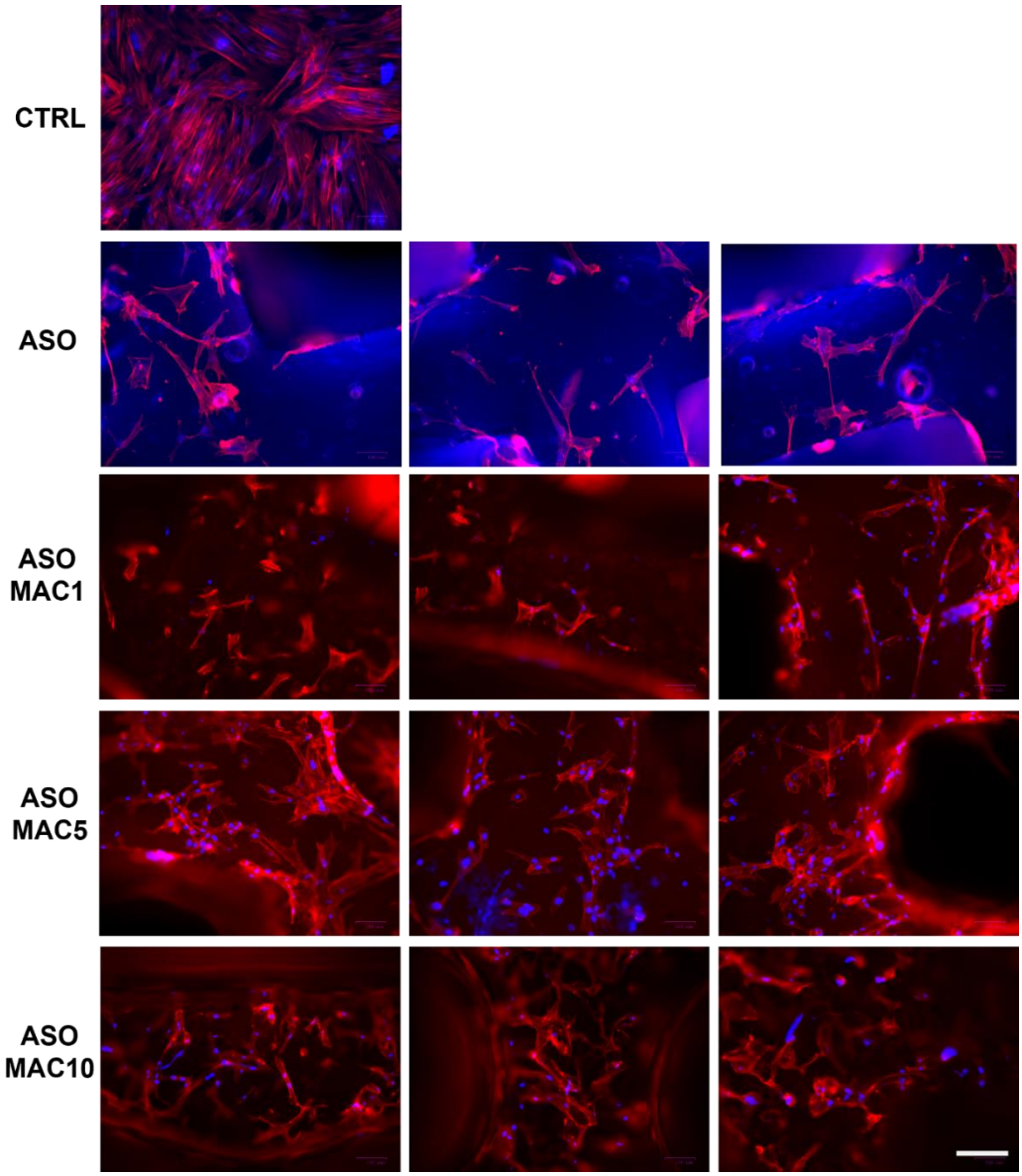


## Conclusions

Innovative biobased composites based on acrylated soybean oil and macadamia nutshell powder as reinforcing agent were successfully prepared *via* DLP-printing. IR

spectroscopy and photorheology and confirmed the high reactivity of the ASO-MAC formulations, while evidencing a slight UV-shielding effect in the formulations containing MAC. Indeed, fast curing kinetic and high double bond conversion (DBC > 85%) were observed for all the formulations being investigated. Subsequently, the excellent DLP-printability was illustrated as complex 3D geometries were successfully reproduced with high resolution, as proved with optical microscopy. The thermomechanical investigation showed that increasing MAC content induced an enhancement of Tg of the composites (increasing from 25 to 46°C) Moreover, the MAC addition led to the formation of stiffer thermosets with an increased Young's modulus (up to +660%, increase). FESEM analyses further confirmed the good dispersion of the MAC particles in the ASO matrix. Finally, the promising cell adhesion and proliferation tests envisage potential applications in biomedical field, including fabrication of scaffolds for tissue engineering.

**Founding**

This research did not receive any specific grant from funding agencies in the public, commercial, or not-for-profit sectors.

## CRediT authorship contribution statement

**Camilla Noè:** Investigation, Methodology, Writing – original draft, editing: **Andrea Cosola:** Writing, 3D-printing investigation, Review. **Chiara Tonda-Turo:** Cell tests, Review. **Raffaella Sesana:** Review. **Cristina Delprete:** Review. **Annalisa Chiappone:** Review. **Minna Hakkarainen:** Review, Supervision. **Marco Sangermano:** Review, Supervision.

## Declaration of Competing Interest

The authors declare no conflict of interest

## References


[1] M. Analysis, T. Filaments, M. Powders, M. Wire, IDTechEx Research : 3D printing materials market worth $ 23B in 2029, (2019) 10–11.

[2] N. Löwa, J.M. Fabert, D. Gutkelch, H. Paysen, O. Kosch, F. Wiekhorst, 3D-printing of novel magnetic composites based on magnetic nanoparticles and photopolymers, Journal of Magnetism and Magnetic Materials. 469 (2019) 456–460. https://doi.org/10.1016/j.jmmm.2018.08.073.

[3] A. Medellin, W. Du, G. Miao, J. Zou, Z. Pei, C. Ma, Vat photopolymerization 3d printing of nanocomposites: A literature review, Journal of Micro and Nano-Manufacturing. 7 (2019). https://doi.org/10.1115/1.4044288.

[4] V.S.D. Voet, J. Guit, K. Loos, Sustainable Photopolymers in 3D Printing: A Review on Biobased, Biodegradable, and Recyclable Alternatives, Macromolecular Rapid Communications. 42 (2021) 1–11. https://doi.org/10.1002/marc.202000475.

[5] A. Cosola, R. Conti, H. Grützmacher, M. Sangermano, I. Roppolo, C.F. Pirri, A. Chiappone, Multiacrylated Cyclodextrin: A Bio-Derived Photocurable Macromer for VAT 3D Printing, Macromolecular Materials and Engineering. 305 (2020) 1–6. https://doi.org/10.1002/mame.202000350.

[6] C. Noè, C. Tonda-Turo, A. Chiappone, M. Sangermano, M. Hakkarainen, Light processable starch hydrogels, Polymers. 12 (2020) 1359. https://doi.org/10.3390/POLYM12061359.

[7] J. Yang, X. An, L. Liu, S. Tang, H. Cao, Q. Xu, H. Liu, Cellulose, hemicellulose, lignin, and their derivatives as multi-components of bio-based feedstocks for 3D printing, Carbohydrate Polymers. 250 (2020) 116881. https://doi.org/10.1016/j.carbpol.2020.116881.

[8] E. Sanchez-Rexach, T.G. Johnston, C. Jehanno, H. Sardon, A. Nelson, Sustainable Materials and Chemical Processes for Additive Manufacturing, Chemistry of Materials. 32 (2020) 7105–7119. https://doi.org/10.1021/acs.chemmater.0c02008.

[9] C. Noè, M. Hakkarainen, M. Sangermano, Cationic uv-curing of epoxidized biobased resins, Polymers. 13 (2021) 1–16. https://doi.org/10.3390/polym13010089.

[10] S. Malburet, D. Mauro, C. Noè, A. Mija, Sustainable access to fully biobased epoxidized vegetable oil thermoset materials prepared by thermal or UV-cationic processes, RSC Advances. (2020) 41954–41966. https://doi.org/10.1039/d0ra07682a.

[11] C. Noè, L. Iannucci, S. Malburet, A. Graillot, M. Sangermano, S. Grassini, New UV-Curable Anticorrosion Coatings from Vegetable Oils, Macromolecular Materials and Engineering. 2100029 (2021) 2100029. https://doi.org/10.1002/mame.202100029.

[12] H. Uyama, M. Kuwabara, T. Tsujimoto, S. Kobayashi, Enzymatic synthesis and curing of biodegradable epoxide-containing polyesters from renewable resources, Biomacromolecules. 4 (2003) 211–215. https://doi.org/10.1021/bm0256092.

[13] R.L. Shogren, Z. Petrovic, Z. Liu, S.Z. Erhan, Biodegradation behavior of some vegetable oil-based polymers, Journal of Polymers and the Environment. 12 (2004) 173–178. https://doi.org/10.1023/B:JOOE.0000038549.73769.7d.

[14] D. Behera, A.K. Banthia, Synthesis, characterization, and kinetics study of thermal decomposition of epoxidized soybean oil acrylate, Journal of Applied Polymer Science. 109 (2008) 2583–2590. https://doi.org/10.1002/app.28350.

[15] S. Miao, W. Zhu, N.J. Castro, M. Nowicki, X. Zhou, H. Cui, J.P. Fisher, L.G. Zhang, 4D printing smart biomedical scaffolds with novel soybean oil epoxidized acrylate, Scientific Reports. 6 (2016) 1–10. https://doi.org/10.1038/srep27226.

[16] M. Lebedevaite, J. Ostrauskaite, E. Skliutas, M. Malinauskas, Photoinitiator free resins composed of plant-derived monomers for the optical μ-3D printing of thermosets, Polymers. 11 (2019). https://doi.org/10.3390/polym11010116.

[17] J. Guit, M.B.L. Tavares, J. Hul, C. Ye, K. Loos, J. Jager, R. Folkersma, V.S.D. Voet, Photopolymer Resins with Biobased Methacrylates Based on Soybean Oil for Stereolithography, ACS Applied Polymer Materials. 2 (2020) 949–957. https://doi.org/10.1021/acsapm.9b01143.

[18] S.D. Silbert, P. Simpson, R. Setien, M. Holthaus, J. la Scala, C.A. Ulven, D.C. Webster, Exploration of Bio-Based Functionalized Sucrose Ester Resins for Additive Manufacturing via Stereolithography, ACS Applied Polymer Materials. 2 (2020) 2910–2918. https://doi.org/10.1021/acsapm.0c00417.

[19] W. Xu, S. Jambhulkar, Y. Zhu, D. Ravichandran, M. Kakarla, B. Vernon, D.G. Lott, J.L. Cornella, O. Shefi, G. Miquelard-Garnier, Y. Yang, K. Song, 3D printing for polymer/particle-based processing: A review, Composites Part B: Engineering. 223 (2021) 109102. https://doi.org/10.1016/j.compositesb.2021.109102.

[20] E.B. Joyee, L. Lu, Y. Pan, Analysis of mechanical behavior of 3D printed heterogeneous particle-polymer composites, Composites Part B: Engineering. 173 (2019). https://doi.org/10.1016/j.compositesb.2019.05.051.

[21] V. Mazzanti, L. Malagutti, F. Mollica, FDM 3D printing of polymers containing natural fillers: A review of their mechanical properties, Polymers. 11 (2019). https://doi.org/10.3390/polym11071094.

[22] N.E. Zander, J.H. Park, Z.R. Boelter, M.A. Gillan, Recycled Cellulose Polypropylene Composite Feedstocks for Material Extrusion Additive Manufacturing, ACS Omega. 4 (2019) 13879–13888. https://doi.org/10.1021/acsomega.9b01564.

[23] F. Fan, Z. Yang, H. Li, Z. Shi, H. Kan, Preparation and properties of hydrochars from macadamia nut shell via hydrothermal carbonization, Royal Society Open Science. 5 (2018). https://doi.org/10.1098/rsos.181126.

[24] S.L.B. Navarro, C.E.C. Rodrigues, Macadamia oil extraction methods and uses for the defatted meal byproduct, Trends in Food Science and Technology. 54 (2016) 148–154. https://doi.org/10.1016/j.tifs.2016.04.001.

[25] R. Sesana, C. Delprete, M. Sangermano, Mechanical behavior of macadamia nutshells, Procedia Structural Integrity. 24 (2019) 829–836. https://doi.org/10.1016/j.prostr.2020.02.088.

[26] J. Girdis, L. Gaudion, G. Proust, S. Löschke, A. Dong, Rethinking Timber: Investigation into the Use of Waste Macadamia Nut Shells for Additive Manufacturing, Jom. 69 (2017) 575–579. https://doi.org/10.1007/s11837-016-2213-6.

[27] R.P. Wool, 15 - NANOCLAY BIOCOMPOSITES, in: R.P. Wool, X.S.B.T.-B.-B.P. and C. Sun (Eds.), Academic Press, Burlington, 2005: pp. 523–550. https://doi.org/https://doi.org/10.1016/B978-012763952-9/50016-2.

[28] L. Bryen, I. Mcconachie, N. Vock, Macadamia Variety Identifier, Agriculture. (1998).

[29] C. Delprete, R. Sesana, Mechanical characterization of kernel and shell of hazelnuts: Proposal of an experimental procedure, Journal of Food Engineering. 124 (2014) 28–34. https://doi.org/10.1016/j.jfoodeng.2013.09.027.

[30] P. Specimens, T. Specimens, Standard Test Method for Tensile Properties of Plastics By Use of Microtensile, 08 (2002) 1–5. https://doi.org/10.1520/D1708-18.2.

[31] E.M. Wilts, A. Gula, C. Davis, N. Chartrain, C.B. Williams, T.E. Long, Vat photopolymerization of liquid, biodegradable PLGA-based oligomers as tissue scaffolds, European Polymer Journal. 130 (2020) 109693. https://doi.org/10.1016/j.eurpolymj.2020.109693.

[32] A. Cortés, A. Cosola, M. Sangermano, M. Campo, S. González Prolongo, C.F. Pirri, A. Jiménez-Suárez, A. Chiappone, Development of 3D printable formulations containing CNT with enhanced electrical properties, Advanced Functional Materials. 31 (2021) 2106774. https://doi.org/10.1016/j.polymer.2016.12.051.

[33] A. Cortés, A. Cosola, M. Sangermano, M. Campo, S. González Prolongo, C.F. Pirri, A. Jiménez-Suárez, A. Chiappone, DLP 4D-Printing of Remotely Modularly and Selectively Controllable Shape Memory.pdf, Advanced Functional Materials. 31 (2021) 2106774. https://onlinelibrary.wiley.com/doi/10.1002/adfm.202106774.

[34] E. Bayarsaikhan, J.H. Lim, S.H. Shin, K.H. Park, Y.B. Park, J.H. Lee, J.E. Kim, Effects of postcuring temperature on the mechanical properties and biocompatibility of three-dimensional printed dental resin material, Polymers. 13 (2021). https://doi.org/10.3390/polym13081180.

[35] J. Li, C. Wu, P.K. Chu, M. Gelinsky, 3D printing of hydrogels: Rational design strategies and emerging biomedical applications, Materials Science and Engineering R: Reports. 140 (2020). https://doi.org/10.1016/j.mser.2020.100543.

[36] J.H. Park, H. Lee, J.W. Kim, J.H. Kim, Cytocompatibility of 3D printed dental materials for temporary restorations on fibroblasts, BMC Oral Health. 20 (2020) 1–9. https://doi.org/10.1186/s12903-020-01150-2.

[37] G.P. Simon, P.E.M. Allen, D.R.G. Williams, Properties of dimethacrylate copolymers of varying crosslink density, Polymer. 32 (1991) 2577–2587. https://doi.org/10.1016/0032-3861(91)90337-I.

[38] G. Savini, R.L. Oréfice, Comparative study of HDPE composites reinforced with microtalc and nanotalcs: high performance filler for improving ductility at low concentration levels, Journal of Materials Research and Technology. 9 (2020) 16387–16398. https://doi.org/10.1016/j.jmrt.2020.11.090.

[39] Y. Zamani, G. Amoabediny, J. Mohammadi, H. Seddiqi, M.N. Helder, B. Zandieh-Doulabi, J. Klein-Nulend, J.H. Koolstra, 3D-printed poly(Ɛ-caprolactone) scaffold with gradient mechanical properties according to force distribution in the mandible for mandibular bone tissue engineering, Journal of the Mechanical Behavior of Biomedical Materials. 104 (2020) 103638. https://doi.org/10.1016/j.jmbbm.2020.103638.

[40] S.-F. Wang, Y.-C. Wu, Y.-C. Cheng, W.-W. Hu, The Development of Polylactic Acid/Multi-Wall Carbon Nanotubes/Polyethylene Glycol Scaffolds for Bone Tissue Regeneration Application, Polymers. 13 (2021) 1740. https://doi.org/10.3390/polym13111740.

[41] C.F. Guimarães, L. Gasperini, A.P. Marques, R.L. Reis, The stiffness of living tissues and its implications for tissue engineering, Nature Reviews Materials. 5 (2020) 351–370. https://doi.org/10.1038/s41578-019-0169-1.

[42] S.C. Zunjarrao, R.P. Singh, Characterization of the fracture behavior of epoxy reinforced with nanometer and micrometer sized aluminum particles, Composites Science and Technology. 66 (2006) 2296–2305. https://doi.org/10.1016/j.compscitech.2005.12.001.